

SCIENTIFIC REPORTS



OPEN

Highly wear-resistant and low-friction Si_3N_4 composites by addition of graphene nanoplatelets approaching the 2D limit

Received: 12 April 2017

Accepted: 7 August 2017

Published online: 30 August 2017

Orsolya Tapasztó¹, Ján Balko², Viktor Puchy², Péter Kun¹, Gergely Dobrik¹, Zsolt Fogarassy¹, Zsolt Endre Horváth¹, Ján Dusza², Katalin Balázsi¹, Csaba Balázsi¹ & Levente Tapasztó¹

Graphene nanoplatelets (GNPs) have emerged as one of the most promising filler materials for improving the tribological performance of ceramic composites due to their outstanding solid lubricant properties as well as mechanical and thermal stability. Yet, the addition of GNPs has so far enabled only a very limited improvement in the tribological properties of ceramics, particularly concerning the reduction of their friction coefficient. This is most likely due to the challenges of achieving a continuous lubricating and protecting tribo-film through a high GNP coverage of the exposed surfaces. Here we demonstrate that this can be achieved by efficiently increasing the exfoliation degree of GNPs down to the few-layer (FL) range. By employing FL-GNPs as filler material, the wear resistance of Si_3N_4 composites can be increased by more than twenty times, the friction coefficient reduced to nearly its half, while the other mechanical properties are also preserved or improved. Confocal Raman spectroscopy measurements revealed that at the origin of the spectacular improvement of the tribological properties is the formation of a continuous FL-GNP tribo-film, already at 5 wt% FL-GNP content.

The outstanding wear resistance of ceramic materials is exploited in a wide range of technological applications. For contact mechanical applications (e.g. bearings, valves) the high wear resistance is desirable to be also associated with a low friction coefficient. Significantly decreasing the friction coefficient is essential for reducing the losses in moving and rotating parts, while increasing the wear resistance improves the durability and lifetime of the components. It is also particularly important, that these benefits come without compromising the other mechanical properties such as toughness, hardness or flexural strength of the composite. The addition of layered materials, known as excellent solid lubricants, is a promising strategy to improve both the mechanical and tribological performance of ceramics. Graphene nanoplatelets have emerged as a particularly promising nanoscale filler phase for various composite materials due to their exceptional mechanical properties and thermal stability¹. They also hold the potential for improving the tribological properties of the composites as graphite is known to be an excellent solid lubricant².

The research conducted so far on the effect of GNP addition on the tribological properties of ceramic materials indicates that the results are strongly dependent on the type of the ceramic matrix. A significant increase (about an order of magnitude) in the wear resistance has been reported for Al_2O_3 ³ and SiO_2 matrix composites⁴. By contrast, for other technologically relevant ceramic materials, such as SiC ⁵, Si_3N_4 ⁶ and ZrO_2 composites⁷ only a moderate 50–70% improvement of the wear rate could be achieved. Concerning the reduction of the friction coefficient, the GNP addition so far has proven even less effective, in several cases the stationary friction coefficient of the ceramic/GNP composites increased or the reduction was only marginal. The most promising results again have been reported for Al_2O_3 where a friction coefficient reduction of up to 20–30% could be achieved³.

In the present work we focus on the tribological properties of Si_3N_4 /GPN composites. Although the addition of GNPs has brought spectacular results in improving the electrical conductivity⁸ and enhancing the fracture

¹Institute of Technical Physics and Materials Science, Centre for Energy Research, Hungarian Academy of Sciences, Konkoly Thege str. 29–33, 1121, Budapest, Hungary. ²Institute of Materials Research, Slovak Academy of Sciences, Watsonova 47, 040 01, Kosice, Slovak Republic. Correspondence and requests for materials should be addressed to L.T. (email: tapaszto@mfa.kfki.hu)

toughness^{9,10} of Si_3N_4 composites, improving the tribological properties has proven particularly challenging. Belmonte *et al.* reported the improvement of the wear resistance up to 56% for Si_3N_4 ceramics prepared by spark plasma sintering (SPS) with 3 wt% GNP addition¹¹. Due to the GNP addition, the friction coefficient increased for loads below 100 N, while a slight reduction of friction could be observed at 200 N, under isoctane lubricated conditions. The elastic modulus, hardness, and fracture toughness of the 3 wt% GNPs composites has slightly decreased as compared to the monolithic material. For Si_3N_4 samples sintered by hot isostatic pressing (HIP) with 3 wt% of GNP addition Hvizdos *et al.* reported a 60% increase of the wear resistance under dry sliding conditions; however, the friction coefficient remained practically unchanged⁶. Hot pressed Si_3N_4 /GNP composites with up to 10 wt% GNP content investigated by Rutkowsi *et al.* displayed an increasing wear rate and friction coefficient with GNP content above 2 wt%, while the other mechanical properties of the composites have also declined¹². Recently, a detailed study has been conducted with our participation on the tribological properties of the Si_3N_4 /GNP composites, prepared by both SPS and HIP methods¹³. Only a limited improvement of the tribological properties could be achieved. Our conclusion was that this is most likely due to lack of formation of a continuous GNP-based lubricant film on the composite surfaces. Recently Si_3N_4 composites with 2 wt% of boron nitride nanoplatelets addition have been prepared by hot pressing¹⁴. Such composites displayed about 20% of reduction in the friction coefficient as compared to monolithic Si_3N_4 .

The picture unfolding from the results concerning the tribological performance of the Si_3N_4 /GNP composites is a moderate improvement of the wear resistance while the friction coefficient is often increased or only marginally reduced. This is in striking contrast with the expectations based on the excellent solid lubricant properties of graphite, which are expected to be inherited also by GNPs. It has been shown that the lubricating properties of graphite are preserved down to four layers, after which the friction gradually increases as the number of layers is further reduced³. As the usually applied GNPs have a thickness of orders of tens of graphene layers, this is clearly not a limiting factor. However, Scanning Electron Microscopy (SEM) and Raman analysis of the wear tracks revealed the lack of a continuous GNP tribo-film formation^{6,11,13} that is at the origin of the limited improvement in the tribological performance. The reason for this is the relatively low GNP coverage of the contact surfaces. This is surprising, as graphene is characterized by an enormous surface area up to $2630 \text{ m}^2/\text{g}$ in the single layer limit. This means that already a few percent of graphene content, if homogeneously distributed within the volume of the composite matrix, easily enables a quasi-continuous coverage of practically any composite surface. The fact that the continuous GNP coverage is still difficult to achieve is most likely due to the low exfoliation level of GNPs, yielding a thickness distribution far from the two dimensional limit, and a much lower surface to volume ratio of the GNPs. A straightforward solution of this problem is increasing the exfoliation degree of GNPs.

Various exfoliation methods have been employed aiming to produce large quantities of single and few layer graphene flakes with their structure kept as intact as possible. The chemical route is highly efficient in improving the exfoliation degree of graphite¹⁵. However, it provides graphene oxide layers, which have been found to be far less effective in improving the mechanical and tribological properties of ceramic composites, even in their reduced form, as compared to chemically unaltered graphene^{3,5}. The liquid phase exfoliation of graphite¹⁶ is a promising route towards obtaining few layer graphene sheets with noncovalent functionalization; however the yield of thick multilayer flakes is relatively high. Here we employ a simple mechanochemical exfoliation method based on the ball milling of graphite with melamine addition to increase the exfoliation efficiency. The efficiency of the melamine has been attributed to the fact that it can easily intercalate graphite and form large 2D networks in-between the graphite layers, weakening the van der Waals forces between them that in turn allows an easy exfoliation upon mild shear stress during ball milling^{17,18}. Although, the method has been originally developed to provide stable water dispersions of few-layer graphene sheets, we show that FL-GNPs produced this way, can be highly efficient filler materials for ceramic composites, especially regarding the improvement of the tribological properties.

Experimental

The graphene nanoplatelets have been exfoliated from commercial graphite powder (Aldrich) by attritor milling (Union Process, type 01-HD/HDDM) for 10 h at 3000 rpm in ethanol¹⁹. After milling, 30 mg of the as-prepared GNPs were introduced in a planetary mill (ZrO_2 balls), with 90 mg of commercially available melamine (Aldrich) addition, and ball-milled at 225 rpm for 30 minutes. The resulting solid mixtures were dispersed in 20 ml water and sonicated for 30 min. For silicon nitride preparation, 90 wt% Si_3N_4 (Ube, SN-ESP) has been used as starting powder, while as sintering aids we used 4 wt% Al_2O_3 (Alcoa, A16) and 6 wt% Y_2O_3 (H.C. Starck, grade C) powders. The powder mixtures were milled in ethanol using an attritor mill (Union Process, type 01-HD/HDDM) at 4000 rpm for 5 h, in a silicon nitride tank, using ZrO_2 balls. 3 and 5 wt% of exfoliated FL-GNPs (preparation process described above) have been added to the batches and homogenized by mechanical milling at 600 rpm for 30 minutes. We chose 3 wt% and 5 wt% of FL-GNPs addition to allow comparison with previous works available on Si_3N_4 /GNP composites with similar compositions^{6,11,13}. The as-prepared powder mixtures have been subjected to spark plasma sintering (SPS, HD P5, FCT - SYSTEME GMBH). The mixtures were sintered into discs of 3 cm in diameter and 5 mm thickness, at 1700 °C in vacuum, with 10 min dwell time. See Methods section for further details of preparation and investigations. The tribological measurements have been performed using a Si_3N_4 ball ($D = 6 \text{ mm}$) under dry sliding conditions, with 5 N loading and 10 cm/s sliding speed. Before the tribological measurements the sample surfaces have been polished down to down to a surface roughness below $\text{Ra} = 0.05 \mu\text{m}$ for the monolithic Si_3N_4 . For composites containing nanoplatelets this was not possible, due to residual porosity. In this case we measured the average roughness after polishing by optical interferometry, yielding values of $\text{R}_a = 0.055 - 0.066 \mu\text{m}$.

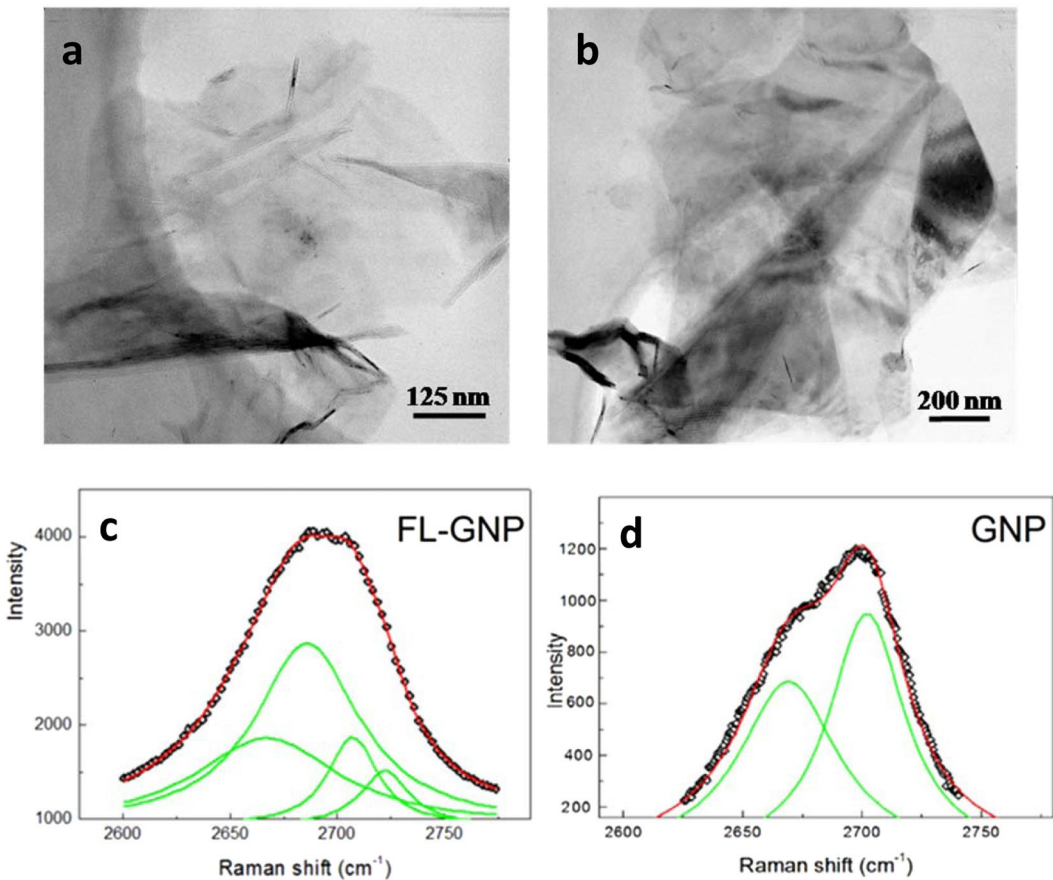


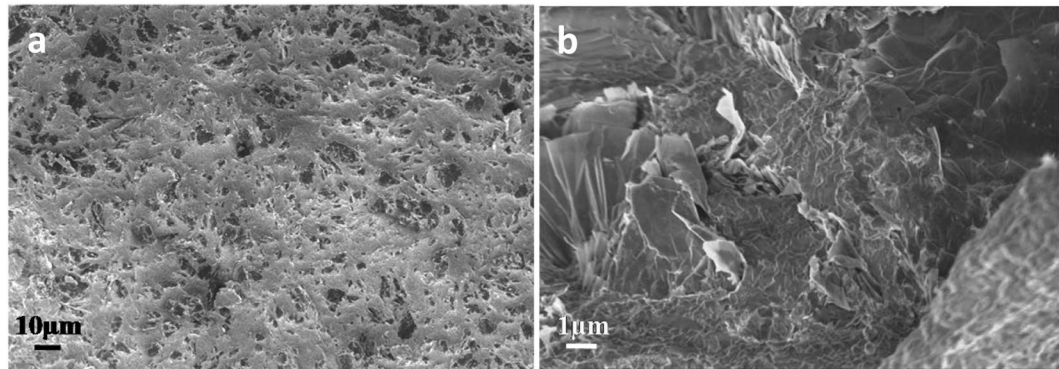
Figure 1. Transmission electron microscopy images of graphene nanoplatelets exfoliated by mechanical milling with melamine addition, resulting in substantially thinner few-layer GNPs (a) as compared to those obtained by conventional exfoliation (b). The analysis of the corresponding 2D Raman peaks confirms the few-layer nature of the graphene nanoplatelets prepared by melamine addition (c), in contrast to the bulk graphitic nature of GNPs prepared without melamine (d).

Results and Discussions

To investigate the efficiency of the applied exfoliation method and the structure of the resulting GNPs we have performed TEM measurements on GNP samples prepared by the very same exfoliation process (see experimental section) both with and without melamine addition. Two characteristic TEM images are shown in Fig. 1. From the TEM investigations it becomes evident that the GNPs prepared by melamine addition are significantly thinner than the conventionally exfoliated GNPs. We estimate that the presence of melamine during milling reduces the average platelet thickness below 10 layers. By contrast, conventionally prepared GNPs typically consist of 40–60 layers. We have also performed Raman spectroscopy to further characterize the thickness of the exfoliated graphene nanoplatelets. The shape of the 2D peak is one of the most widely used parameters that correlates with the layer thickness in the few-layer limit²⁰. Up to four layers, the layer number can be precisely determined²⁰ from the 2D peak shape. Above four layers, the precise layer number cannot be reliably extracted; however, the shape of the 2D peak is still distinguishable from that of bulk graphite up to above ten layers^{21,22}. From Fig. 1c,d it is apparent that the 2D peak of the samples exfoliated with melamine addition (FL-GNPs) is clearly different from that of bulk graphite (>10 layers), while the GNPs exfoliated without melamine closely resemble the 2D peak of graphite, in good agreement with the TEM findings. For graphene nanoplatelets prepared by melamine addition the 2D peak can be fitted by multiple Lorentzian peaks, which is characteristic to few-layer graphene samples^{21,22}. For further analysis of the Raman spectra see SI. Consequently TEM and Raman investigations clearly indicate that melamine addition highly enhances the exfoliation efficiency of graphene nanoplatelets during ball milling, reducing their thickness in the few-layer (<10 layers) range, in full agreement with the literature on melamine enhanced exfoliation of graphite^{17,18}.

Nevertheless, even in the case of melamine addition, we only approach but typically do not reach the 2D limit, namely, single graphene layers. However, this is an advantage for tribological applications, as platelets below 4 layers are characterized by diminished lubricating properties¹⁵. The advantage of using melamine is its non-invasive nature; it does not form strong chemical bonds to the graphene scaffold that would modify its electrical and mechanical properties¹⁷. We confirm this by Raman spectroscopy investigations of the resulting FL-GNPs that display a relatively small D peak (mainly attributed to flake edges), indicative of high structural quality of the FL-GNPs (see Figs S1 and S2 of SI). After the exfoliation by milling, the melamine can be removed using hot

Material	App. Density (g/cm ³)	$\alpha\text{-Si}_3\text{N}_4$ (%)	$\beta\text{-Si}_3\text{N}_4$ (%)	ZrO ₂ (%)
Si ₃ N ₄	3.32	38,6	58,7	2,4
Si ₃ N ₄ /3%GNP	3.28	40,1	54,3	2,1
Si ₃ N ₄ /3%FL-GNP	3.3	60	33,2	1,1
Si ₃ N ₄ /5%FL-GNP	3.13	53,2	36,7	2,1

Table 1. The apparent density and phase composition of Si₃N₄/GNP composites.**Figure 2.** Scanning electron microscopy images of fracture surfaces of Si₃N₄ composites with 5 wt% of FL-GNP addition. (a) Lower magnification images reveal a relatively high surface density of micron-scale dark areas that can be identified in higher resolution SEM images (b) as few-layer graphene nanoplatelets lying flat on the surface.

water, leaving behind the pure FL-GNP powder. Potential melamine residues are fully removed during the sintering process at 1600 °C, as melamine decomposes over 350 °C²³.

The microstructure of the sintered Si₃N₄/FL-GNP composites has been investigated by Scanning Electron Microscopy (SEM) and XRD. The structural data obtained from XRD measurements (Fig. S4 SI) are summarized in Table 1. The average Si₃N₄ grain size from SEM investigations was found to be about 280 +/− 20 nm for monolithic Si₃N₄, and about 250 +/− 20 nm for composites with nanoplatelet additions. Lower magnification SEM images (Fig. 2a) display a relatively high density of darker areas with micron-scale characteristic lateral size. Higher magnifications (Fig. 2b) reveal that these areas are not GNP aggregates, but FL-GNPs lying parallel on the surface of the Si₃N₄ composite. Indeed, even few-layer graphene sheets can give a substantial contrast in SEM images when lying flat on insulating substrates²⁴. Although SEM measurements more easily detect larger area flakes, the lateral size of the FL-GNPs varies from a few hundred nanometers to several microns. From higher resolution SEM images, FL-GNPs oriented both parallel and perpendicular to the surface can be identified, which is in contrast to the SEM images most often reported in the literature, where usually only a few FL-GNPs perpendicular to the surface can be identified. We attribute this to the much higher surface area covered by FL-GNPs as compared to their thicker GNP counterparts. It is also known that sintering processes employing uniaxial pressure yield GNPs with a preferential orientation perpendicular to the pressure axis²⁵. Nevertheless, we observed a high concentration of GNPs in SEM images acquired on various fracture surfaces. This can be attributed to the partial nature of the FL-GNP alignment and a high FL-GNP density ensuring the presence of platelets parallel to various fracture surfaces.

Figure 3 shows the friction coefficient of various composites acquired under the same experimental conditions (see Experimental section). The addition of 3 wt% of conventional GNP exfoliated without melamine addition results in a friction coefficient of 0.79 +/− 0.02, practically identical to that of the monolithic Si₃N₄. This is consistent with our previous results, as well as the reports from the literature^{6,11}. The addition of 3 wt% of FL-GNPs exfoliated with melamine addition results in a roughly 15% reduction of the friction coefficient. However, the most exciting results have been obtained for 5 wt% of FL-GNP addition, where the steady state friction coefficient was found 0.43 +/− 0.04, almost half of the value for monolithic Si₃N₄. To our knowledge such a substantial reduction of the friction coefficient upon GNP addition has not been reported before in Si₃N₄ or any other ceramic composite. It is also worth noting that in contrast to monolithic and 3 wt% GNP samples, for samples with FL-GNP addition the friction coefficient slightly but steadily decreases as a function of sliding distance. This might indicate the self-lubricating nature of the composite leading to the exposure (pulling out) of more and more FL-GNP flakes, which, together with the high initial FL-GNP surface coverage, further improve the lubricating properties. The wear tracks after 300 m sliding have been investigated by optical microscopy. Figure 4 displays two representative optical images for the monolithic Si₃N₄ and the 5 wt% FL-GNP addition. For the monolithic Si₃N₄ sample a high density of abrasion grooves can be identified, indicative of a severe wearing process. In striking contrast with this, for the 5 wt% FL-GNP composite such abrasion grooves are almost completely absent. Optical images of wear

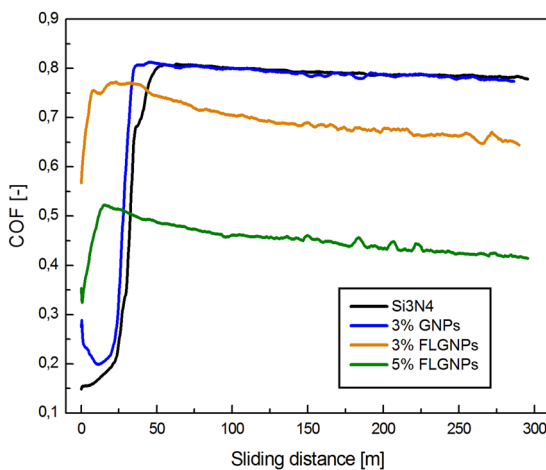


Figure 3. Friction coefficient of various composites measured under dry sliding conditions with Si₃N₄ ball, at 5 N loading, and 10 cm/s sliding speed. Composites with 5 wt% of FL-GNP addition display a highly reduced friction coefficient.

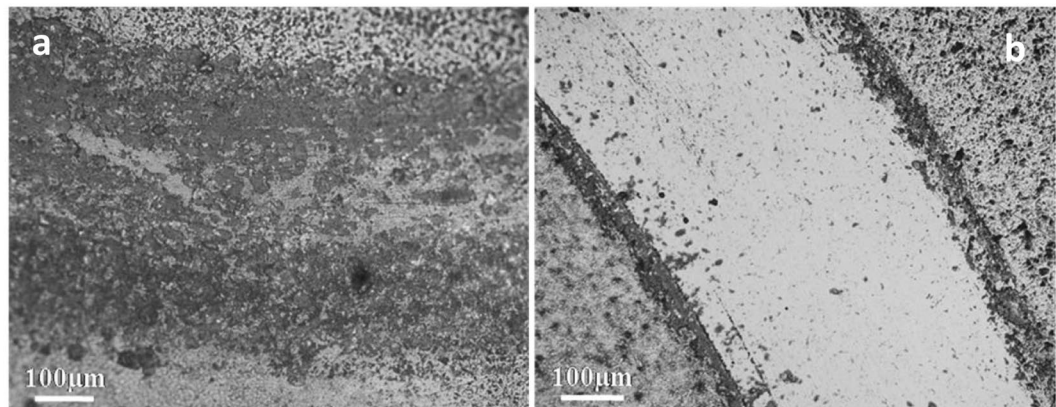


Figure 4. Optical microscopy images of wear tracks for (a) monolithic Si₃N₄ and (b) Si₃N₄/5 wt% FL-GNP composite. While abrasion grooves are present in high density in monolithic samples, they are almost completely absent for the composites with 5 wt% of FL-GNP addition.

tracks for other compositions are shown in Fig. S5 of the SI. The corresponding wear volumes have been measured and the wear rates calculated (Fig. 5a). We found that the wear rate measured for the 5 wt% FL-GNP sample ($5.9 \cdot 10^{-7} \text{ mm}^3/\text{N m}$) is about twenty times lower than the wear rate of the monolithic Si₃N₄ ($1.2 \cdot 10^{-5} \text{ mm}^3/\text{N m}$). This is a spectacular improvement of the wear resistance in full agreement with the optical microscopy images of the wear tracks. For comparison, composites with 3 wt% of GNP display a 14% reduction of wear rate while for the composites with 3 wt% of FL-GNP a 41% reduction has been measured. As concerning the wear rate of the counterpart Si₃N₄ balls for monolithic Si₃N₄ samples a ball wear rate of $1.5 \cdot 10^{-5} \text{ mm}^3/\text{N.m}$ was measured, which is reduced to $1.9 \cdot 10^{-6} \text{ mm}^3/\text{N.m}$ for the 5 wt% FL-GNP/Si₃N₄ sample. We attribute this to the formation of the FL-GNP-based tribo-film protecting also the counterpart ball from wearing (see Fig. S6 of SI).

The outstanding tribological performance achieved for 5 wt% FL-GNP composites can only be fully exploited in technological applications, if this does not come at the expense of other mechanical properties. In order to clarify this we have measured the hardness, three-point bending strength and fracture toughness of the prepared composites on at least three samples. The results are summarized in Fig. 5b. Monolithic S₃N₄ samples display a Vickers hardness of $16.3 \pm 0.4 \text{ GPa}$, their three-point bending strength was found to be $549 \pm 23 \text{ MPa}$, while the fracture toughness $5.0 \pm 0.25 \text{ MPa m}^{1/2}$. As it can be seen for the 3 wt% GNP samples the hardness and bending strength has been slightly decreased while the fracture toughness increased by about 12% in agreement with previous findings^{9,10}. For 3 wt% FL-GNP addition the hardness and flexural strength of the composite has already preserved the values of the monolithic S₃N₄, while the toughness further increased. Finally, for the tribologically best performing 5 wt% FL-GNP sample all the investigated mechanical properties have also been improved. This is most likely due to the fact that a better exfoliation rate leads to a more homogeneous dispersion, as thick GNPs can be regarded as larger aggregates of single layer graphene sheets. Nevertheless, the improvement of the mechanical properties even in this case is moderate, of order of 10–20%. This might be due to the

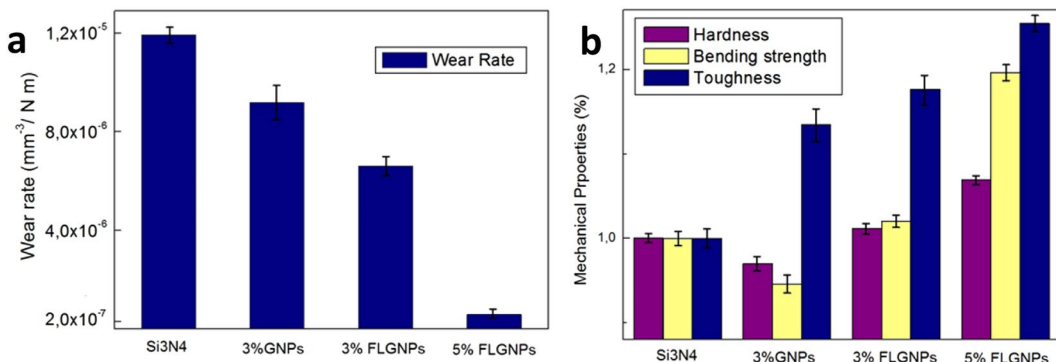


Figure 5. (a) Wear rate of various Si_3N_4 composites displaying a striking improvement of the wear resistance for composites with 5 wt% of FL-GNP addition. (b) The Vickers hardness, three-point bending strength, and fracture toughness of Si_3N_4 composites normalized to the corresponding values of the monolithic Si_3N_4 sample to allow an easy comparison.

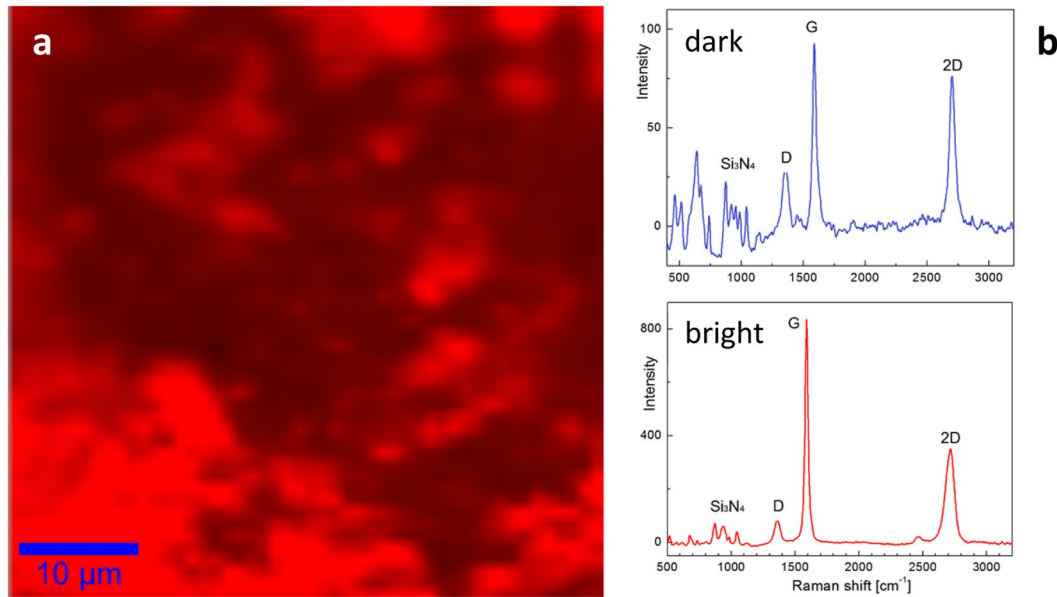


Figure 6. (a) False colored confocal Raman spectroscopy map of the G line of FL-GNPs recorded inside the wear track of a Si_3N_4 /5 wt% FL-GNPs sample. The brightness of the red color indicates the G line intensity. (b) Raman spectra inside the wear track, displaying the main lines of both the FL-GNPs and the Si_3N_4 matrix, characteristic to dark and bright areas of the map.

rather weak interaction between the FL-GNPs and the S_3N_4 ceramic matrix, which on one hand is less efficient for improving the mechanical properties, on the other hand it is beneficial for improving the tribological performance allowing the FL-GNPs embedded in the matrix to be pulled out and incorporated into the tribo-film, leading to the self-lubricating property of the composite.

In order to directly confirm that at the origin of the outstanding tribological properties of 5 wt% FL-GNP composite is indeed the formation of a FL-GNP tribo-film we have performed confocal Raman spectroscopy measurements of the wear tracks. Such Raman mapping has already proven very useful for the characterization of GNP distribution of sample surfaces and wear tracks^{11,26}. A characteristic Raman map is shown in Fig. 6a. The red color symbolizes the presence of G-peak, while the brightness of the color indicates the intensity of the G peak. As can be seen the whole map is red, which indicates that in the wear track FL-GNPs form a continuous film, thought of varying thickness. This is also confirmed by the SEM imaging of the wear tracks (Fig. S7 SI). Raman maps have been acquired on various positions with similar results, indicating that all the investigated wear track areas are covered by a continuous FL-GNP tribo-film. Typical Raman spectra from the bright (thicker) and dark (thinner) areas of the map are shown in Fig. 6b. It is worth noting that even though the intensity ratio of the G and 2D peaks varies with location (see also SI Fig. S2), both spectra acquired in the bright and dark areas display 2D peaks, characteristic to few-layer graphene^{17,21,22}. Another important information that can be obtained from

these Raman spectra is the relatively low intensity of the D peak, indicating that even after the wear process the FL-GNPs preserve their high structural quality.

Conclusions

In summary, we have shown that the addition of graphene nanoplatelets with thickness approaching the two-dimensional limit to Si_3N_4 remarkably improves the tribological performance of such ceramic composites. As compared to monolithic Si_3N_4 , only 5 wt% of few-layer graphene nanoplatelet addition can increase the wear resistance by more than 20 times, while reducing the friction coefficient by 50%. By confocal Raman spectroscopic mapping of the wear tracks we have shown that this outstanding improvement in the tribological properties can be attributed to the formation of a continuous protecting and lubricating tribo-film consisting of FL-GNPs of high structural quality. The hardness, fracture toughness and bending strength of such composites are also improved compared to monolithic Si_3N_4 . There are key technological advantages in developing highly wear-resistant and low-friction ceramic composite materials. Components produced from such materials enable the substantial reduction of losses during operation, as well as a significant increase of their durability in contact mechanical applications.

Methods

The exfoliated FL-GNPs have been investigated by a Philips CM-20 Transmission electron microscope (TEM) at 200 keV and Raman spectroscopy (Witec Alpha 300 RSA).

During the sintering of the composites the powders were heated with $100^\circ\text{C min}^{-1}$ heating rate for all the experiments using on/off current pulses of 12/2, 5500 A and 7.2 V. An applied uniaxial compression of 50 MPa and chamber pressure of 1 mbar has been maintained during sintering. The microstructural characterization of the sintered samples has been carried out by a LEO (ZEISS) 1540 XB field emission scanning electron microscope and XRD measurements (Bruker AXS D8). The wear behaviour of the materials was studied by an unlubricated ball-on-disc setup (ASTM G99-03, Standard test method for wear testing with a pin-on-disk apparatus, 2003) using a tribometer (DTHT 70010, CSM Instrument, Switzerland), against silicon nitride balls (6 mm diameter) with a track radius of 2.5 mm. The Si_3N_4 ball surfaces were ground and polished with a final diamond suspension of $3\ \mu\text{m}$ (roughness $\text{Ra} < 0.25\ \mu\text{m}$). The specimens were tested normal to the major surface of the sample with an applied load of 5 N. The tests were performed in air, at room temperature with a relative humidity of $40 \pm 5\%$. The total sliding distance was 300 m and the sliding velocity was 10 cm/s. The coefficient of friction was continuously recorded during the tests. The wear volume of each specimen was calculated from the surface profile traces (at least 6) across the wear track and perpendicular to the sliding direction using a profilometer (Mitutoyo SJ-201, USA), and by using a high precision confocal microscope (PLuneox 3D Optical Profilometer, Sensofar, Spain). The wear tracks have also been investigated by Raman spectroscopy, using a confocal Raman microscope system (Witec Alpha 300 RSA) with Nd:YAG laser (532 nm, 20 mW). For Raman mapping 2500 spectra have been acquired with 600 lines/mm grating from a $50\ \mu\text{m}$ -wide rectangular area with $1\ \mu\text{m}$ spacing. The bending strength of the composites has been determined by three-point bending tests on a tensile/loading machine (INSTRON-1112). The hardness and fracture toughness values have been obtained from micro-indentation experiments on a hardness tester (KS Prüftechnik) applying a load of 10 Kp for 10 seconds. The fracture toughness was calculated according to the Anstis-formula²⁷, using the Young's modulus value of $E = 250\ \text{GPa}$. For the three-point bending strength measurements the samples have been cut into rectangular specimens of $3.5\ \text{mm} \times 5\ \text{mm} \times 28\ \text{mm}$.

Data availability. The data that support the findings of this study are available from the corresponding author upon request.

References

- Walker, L. S., Marotto, V. R., Rafiee, M. A., Koratkar, N. & Corral, E. L. Toughening in graphene ceramic composites. *ACS Nano* **5**, 182–90 (2011).
- Bollmann, W. & Spreadborough, J. Action of graphite as a lubricant. *Nature* **186**, 29–30 (1960).
- Kim, H. J. *et al.* Unoxidized graphene/alumina nanocomposite: fracture- and wear-resistance effects of graphene on alumina matrix. *Scientific Reports* **4**, 5176 (2014).
- Porwal, H. *et al.* Tribological properties of silica-graphene nano-platelet composites. *Ceramics international* **40**, 12067–12074 (2014).
- Llorente, J., Román-Manso, B., Miranzo, P. & Belmonte, M. Tribological performance under dry sliding conditions of graphene/silicon carbide composites. *Journal of the European Ceramic Society* **36**, 429–435 (2016).
- Hvizdos, P., Dusza, J. & Balázs, C. S. Tribological properties of Si_3N_4 -graphene nanocomposites. *J. Eur. Ceram. Soc.* **33**, 2359–2364 (2013).
- Li, H. *et al.* Microstructure and wear behavior of graphene nanosheets-reinforced zirconia coating. *Ceramics International* **40**, 12821–12829 (2014).
- Ramirez, C., Figueiredo, F. M., Miranzo, P., Poza, P. & Osendi, M. I. Graphene nanoplatelet/silicon nitride composites with high electrical conductivity. *Carbon* **50**, 3607–15 (2012).
- Kvetková, L. *et al.* Fracture toughness and toughening mechanisms in graphene platelet reinforced Si_3N_4 composites. *Scripta Materialia* **66**, 793–796 (2012).
- Ramirez, C. *et al.* Extraordinary toughening enhancement and flexural strength in Si_3N_4 composites using graphene sheets. *J. Eur. Ceram. Soc.* **34**, 161–169 (2014).
- Belmonte, M. *et al.* The beneficial effect of graphene nanofillers on the tribological performance of ceramics. *Carbon* **61**, 431–435 (2013).
- Rutkowski, P. *et al.* The influence of the graphene additive on mechanical properties and wear of hot-pressed Si_3N_4 matrix composites. *J. Eur. Ceram. Soc.* **35**, 87–94 (2015).
- Maros, M. *et al.* Tribological characterisation of silicon nitride/multilayer graphene nanocomposites produced by HIP and SPS technology. *Tribology International* **93**, 269–281 (2016).
- Lee, B., Lee, D., Lee, J. H., Ryu, H. J. & Hong, S. H. Enhancement of toughness and wear resistance in boron nitride nanoplatelet (BNNP) reinforced Si_3N_4 nanocomposites. *Scientific Reports* **6**, 27609 (2016).
- Lee, C. *et al.* Frictional characteristics of atomically thin sheets. *Science* **328**, 76–80 (2010).

16. Hernandez, Y. *et al.* High-yield production of graphene by liquid-phase exfoliation of graphite. *Nature* **3**, 563 (2008).
17. León, V. *et al.* Few-layer graphenes from ball-milling of graphite with melamine. *Chem. Commun.* **47**, 10936–10938 (2011).
18. León, V., Rodriguez, A. M., Prieto, P., Prato, M. & Vázquez, E. Exfoliation of graphite with triazine derivatives under ball-milling conditions: Preparation of few-layer graphene via selective noncovalent interactions. *ACS Nano* **8**, 563–571 (2014).
19. Kun, P. & Wéber, F. Balázsi, Cs. Preparation and examination of multilayer graphene nanosheets by exfoliation of graphite in high efficient attritor mill. *Central European Journal of Chemistry* **9**, 47–51 (2011).
20. Malard, L. M. & Pimeta, M. A. Dresselhaus, g., Dresselhaus, M.S. Raman spectroscopy in graphene. *Phys. Rep.* **473**, 51–87 (2009).
21. Gupta, A., Chen, A., Joshi, P., Tadigadapa, S. & Raman, P. C. scattering from high-frequency phonons in supported n-layer graphene films. *Nano Lett.* **6**, 2667–2673 (2006).
22. Graf, D. *et al.* Spatially resolved Raman spectroscopy of single- and few-layer graphene. *Nano Lett.* **7**, 238–242 (2006).
23. Kapil, P., Rupesh, R. & Cheng, H. Polymeric organo–magnesium complex for room temperature hydrogen physisorption. *RSC Adv.* **5**, 10886–10891 (2015).
24. Kochat, V. *et al.* High contrast imaging and thickness determination of graphene with in-column secondary electron microscopy. *J. Appl. Phys.* **100**, 014315 (2011).
25. Tapasztó, O. *et al.* High orientation degree of graphene nanoplatelets in silicon nitride composites prepared by spark plasma sintering. *Ceramics International* **42**, 1002 (2016).
26. Ramirez, C. & Osendí, M. I. Characterization of graphene nanoplatelets-Si₃N₄ composites by Raman spectroscopy. *J. Eur. Ceram. Soc.* **33**, 471–477 (2013).
27. Anstis, G. R., Chantikul, P., Lawn, B. R. & Marshall, D. B. A critical evaluation or indentation techniques for measuring fracture toughness: I, direct crack measurements. *J. Am. Ceram. Soc.* **64**, 533–538 (1981).

Acknowledgements

O.T. was supported by OTKA grant PD 121368. Funding from the National Research Development and Innovation Office M-ERANET project “Graphene-ceramic composites for tribological application in aqueous environments” is also acknowledged. L.T. acknowledges the ERC Starting Grant, the “Lendület” programme of the Hungarian Academy of Sciences, and OTKA grant K108753.

Author Contributions

O.T. and L.T. conceived and designed the experiments. J.B., V.P. and J.D. performed the sintering and tribology measurements. P.K. and G.D. and L.T. performed the Raman measurements. Z.F. carried out the TEM investigations. H.Z.E performed the XRD measurements. O.T., K.B., C.B. and L.T. analyzed the data. O.T. and L.T. wrote the paper. All authors discussed the results and commented on the manuscript.

Additional Information

Supplementary information accompanies this paper at doi:[10.1038/s41598-017-10290-5](https://doi.org/10.1038/s41598-017-10290-5)

Competing Interests: The authors declare that they have no competing interests.

Publisher's note: Springer Nature remains neutral with regard to jurisdictional claims in published maps and institutional affiliations.



Open Access This article is licensed under a Creative Commons Attribution 4.0 International License, which permits use, sharing, adaptation, distribution and reproduction in any medium or format, as long as you give appropriate credit to the original author(s) and the source, provide a link to the Creative Commons license, and indicate if changes were made. The images or other third party material in this article are included in the article’s Creative Commons license, unless indicated otherwise in a credit line to the material. If material is not included in the article’s Creative Commons license and your intended use is not permitted by statutory regulation or exceeds the permitted use, you will need to obtain permission directly from the copyright holder. To view a copy of this license, visit <http://creativecommons.org/licenses/by/4.0/>.

© The Author(s) 2017